

Catalyst-free highly vertically aligned ZnO nanoneedle arrays grown by plasma-assisted molecular beam epitaxy

J.S. Wang · C.S. Yang · P.I. Chen · C.F. Su · W.J. Chen ·
K.C. Chiu · W.C. Chou

Received: 9 July 2009 / Accepted: 24 September 2009 / Published online: 10 October 2009
© Springer-Verlag 2009

Abstract This work describes the growth of highly vertically aligned ZnO nanoneedle arrays on wafer-scale catalyst-free *c*-plane sapphire substrates by plasma-assisted molecular beam epitaxy under high Zn flux conditions. The photoluminescence spectrum of the as-grown samples reveals strong free exciton emissions and donor-bound exciton emissions with an excellent full width at half maximum (FWHM) of 1.4 meV. The field emission of highly vertically aligned ZnO nanoneedle arrays closely follows the Fowler–Nordheim theory. The turn-on electric field was about 5.9 V/ μ m with a field enhancement factor β of around 793.

PACS 81.07.-b · 81.15.Hi · 79.70.+q

1 Introduction

Recently one-dimensional (1-D) nanostructure materials have stimulated considerable interest because of their novel

fundamental properties and wide range of potential applications in several fields [1–4]. One of their important properties is the high aspect ratio, which makes fascinating candidates for electron field emission since tip geometry is critical to electron field emission properties [5]. The field emitters are useful in high-brightness electron sources and flat panel displays [6]. Among 1-D nanostructure materials, ZnO is an oxide material which is intrinsically resistant to oxidation and has high thermal stability. Therefore, a ZnO-based 1-D nanostructure is an excellent candidate for use in field emission devices and has attracted much attention. ZnO with a wurtzite-structure has a wide direct band gap of 3.37 eV at room temperature and a large exciton binding energy of 60 meV. The fundamental optical properties of ZnO underlie their potential for use in photonic devices [7, 8]. ZnO-based 1-D nanostructures in various forms, including nanowires, nanoneedles and nanopencils, have been grown by various growth methods and examined [9–17]. The results show that electrons are more easily emitted from ZnO nanostructures with sharp tips than from nanowires of uniform diameter. However, ZnO-based 1-D nanostructures grown by molecular beam epitaxy (MBE) have been obtained only using catalyst-driven methods [18, 19].

This work demonstrates the growth of highly vertically aligned ZnO nanoneedle arrays on a wafer-scale catalyst-free *c*-plane sapphire substrate by plasma-assisted molecular beam epitaxy (PA-MBE), and investigates their photoluminescence (PL) and field emission properties.

2 Experiments

The growth was carried out in a Veeco EPI 620 MBE system on a *c*-plane sapphire substrate. An Addon RF-plasma source with independently separated pumping design was

J.S. Wang (✉) · P.I. Chen · C.F. Su · W.J. Chen · K.C. Chiu
Department of Physics, Chung Yuan Christian University,
No. 200, Chung Pei Rd., Chung-Li 32023, Taiwan
e-mail: jswang@cycu.edu.tw

J.S. Wang · K.C. Chiu
Center for Nano-Technology, Chung Yuan Christian University,
Chung-Li 32023, Taiwan

C.S. Yang
Graduate Institute of Electro-Optical Engineering, Tatung
University, Taipei 10452, Taiwan

W.C. Chou
Department of Electrophysics, National Chiao Tung University,
Hsin-Chu 30010, Taiwan

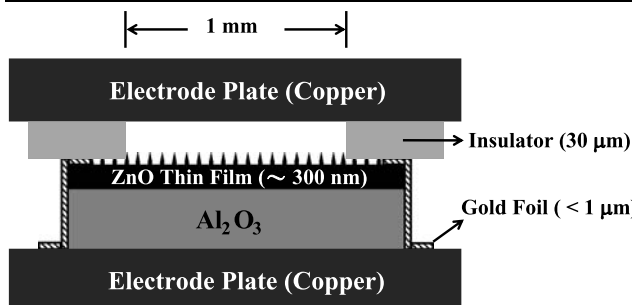


Fig. 1 Schematic diagram of cross-sectional device structure for field emission measurements

used to provide reactive oxygen radicals. The flux of oxygen gas was controlled by a mass flow controller. Knudsen cells were utilized to evaporate the Zn metal source. Before deposition, the substrate was cleaned by acetone and chemically etched using a heated acid solution of H_2SO_4 and H_3PO_4 for 15 min. Thereafter, the substrate was desorbed at 920°C . During growth, the substrate temperature was fixed at 650°C and the oxygen RF-plasma source was kept at 400 W with an oxygen flow rate of 3.0 SCCM. The chamber pressure during growth was around 1×10^{-5} Torr. The entire growth process was monitored by reflection high-energy electron diffraction (RHEED). The surface morphology and film thickness were analyzed using a scanning electron microscope (SEM). The 325 nm line from an He-Cd laser was employed as the exciting source in the PL measurements. The field emission properties of the highly vertically aligned ZnO nanoneedle arrays were measured using a two-parallel-plate configuration in an ultrahigh vacuum chamber with a pressure of better than 1×10^{-7} Torr at room temperature. Figure 1 shows the schematic diagram of cross-sectional device structure. The thickness of flat ZnO layer and the width of device area were about 300 nm and 1 mm, respectively. The gold-foils of thickness less than 1 μm were used for the electrical contact, and therefore the 30 μm -thick plastic insulators determined the electrodes gap.

3 Results and discussion

Recent reports have demonstrated that ZnO thin films grown under stoichiometric and/or slight Zn-rich conditions have flat surface morphologies and better crystalline quality due to better surface migration of the adatoms [20, 21]. Figure 2 plots the growth rate of ZnO thin films, which were estimated from the cross-sectional SEM images, as a function of reciprocal Zn temperature. The flux of the solid source is generally an exponential function of the reciprocal temperature over a suitable range of temperature. As shown in Fig. 2, the growth rate of ZnO thin films rises linearly to near 340°C and then saturates at a higher Zn temperature.

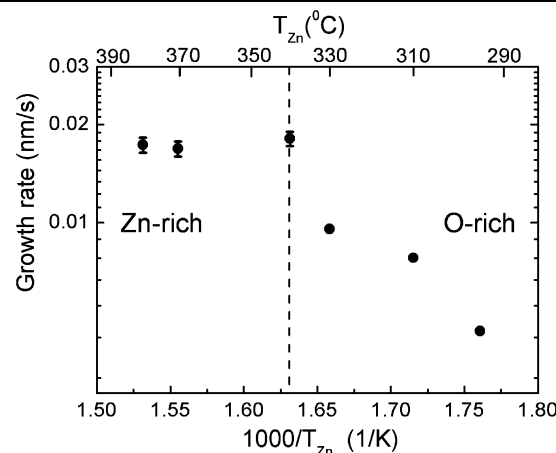


Fig. 2 Growth rates of ZnO thin films at various Zn temperatures under fixed O-plasma conditions, estimated from the cross-sectional SEM images, as a function of reciprocal Zn temperature. The *dashed line* indicates the flat-to-needle transition point

This behavior indicates that the growth mode is limited by the minority atoms on the surface. When the growth rate is governed by O-rich conditions, it linearly increases with the Zn beam flux. When the growth conditions are Zn-rich, the growth rate becomes saturated with further increases in Zn beam flux.

In Fig. 3(a)–(d) present typical SEM images of the sample surfaces which were grown under O-rich toward under Zn-rich conditions. Some island structures with a few vertically aligned nanoneedles were observed on the surface of films at a Zn temperature of 340°C , whereas those samples grown under O-rich conditions had flat surfaces. Highly vertically aligned nanoneedle arrays with average density of around 10^9 cm^{-2} were obtained under high Zn flux conditions. The average length and diameter of needles were about 300 nm and 50 nm, respectively. Hu et al. [22] proposed a model called self-catalyzed vapor–liquid–solid (VLS) growth. They suggested that Zn deposits in the form of liquid droplet and the Zn droplets then react with oxygen to form ZnO. Zn not only acts as a reactant, but also provides an energetically favorable site for the absorption of oxygen. Therefore, no transition metal need be added as a catalyst. Hsu et al. [16] reported a similar conclusion and demonstrated the growth of ZnO nanowires on ZnO : Ga/glass templates at 600°C by a self-catalyzed VLS process. ZnO is well known to be a polar crystal, like GaN, and the polar plane {0001} has higher surface energy than the other non-polar surfaces. Therefore, the crystal growth rate in the {0001} direction is high for energetic reasons under thermodynamic equilibrium conditions [23]. Here strong Zn-rich conditions cause the formation of Zn droplets, and these randomly nucleated Zn droplets act as nucleation sites. The nuclei become larger on the surface and finally grow into 1-D nanoneedle structures. Therefore, the uniformity of the

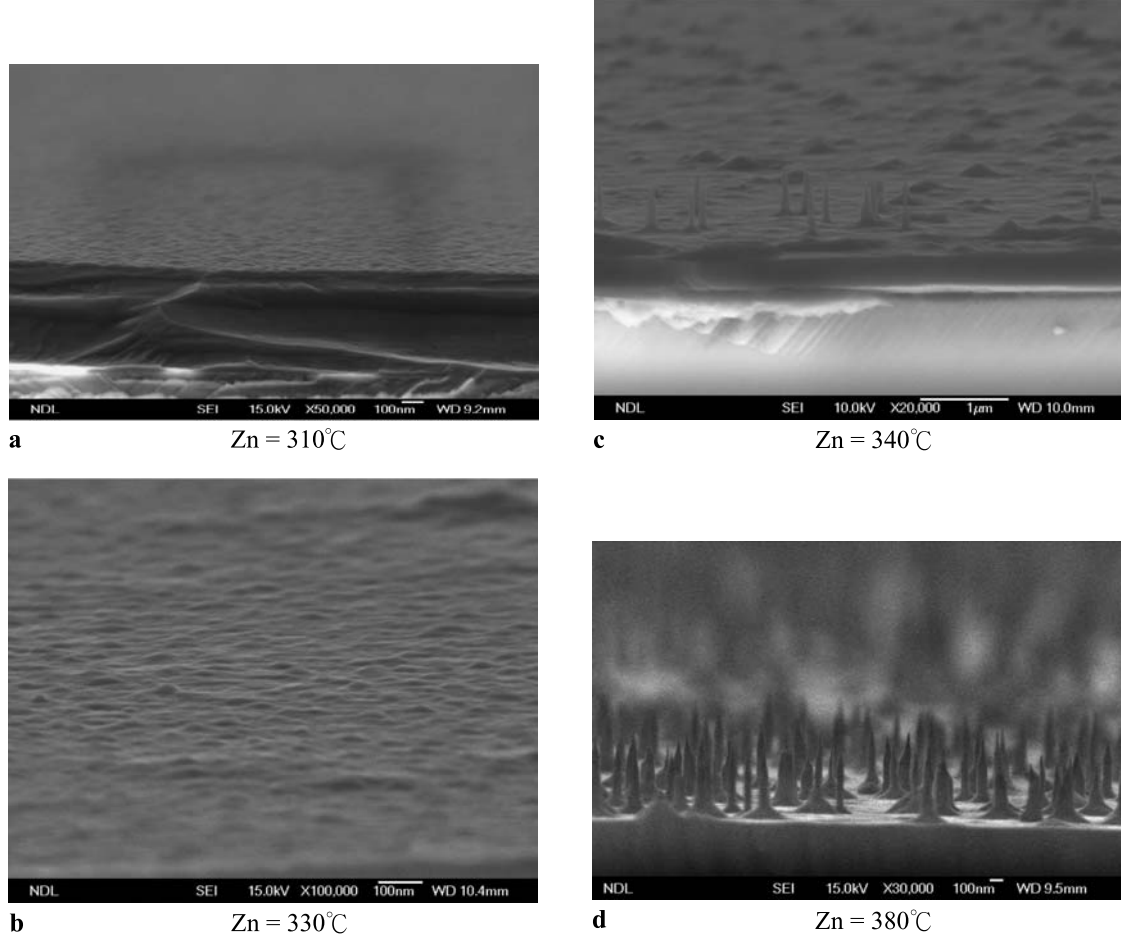


Fig. 3 Typical SEM images of sample surfaces which were grown under O-rich toward Zn-rich conditions, (a) $Zn = 310^{\circ}\text{C}$, (b) $Zn = 330^{\circ}\text{C}$, (c) $Zn = 340^{\circ}\text{C}$, (d) $Zn = 380^{\circ}\text{C}$

nanoneedles probably depends on the uniformity of the Zn droplets, and the random distribution on the surface probably is due to the random nucleation of the Zn droplets.

Figure 4 shows the 10 K PL spectrum of the near-band edge of ZnO nanoneedle arrays. Based on their energy, these emission lines can be ascribed to excitons bound to neutral donors (I_2 , I_4 , I_6 , I_8 and I_9) and free excitons (FX_A and FX_B), respectively [24, 25]. Among them, the dominant peak at 3.358 eV, I_9 , with a full width at half maximum (FWHM) of 1.4 meV is attributable to indium [25]. As shown in Fig. 4, although the PL come not only from the nanoneedles but also the flat base layer, the observation of strong free exciton emissions and bound exciton emissions with excellent FWHM indicates that the samples are of high optical quality.

Figure 5 plots the curve of emission current density (J) as a function of applied electric field (E) for the device area of $1 \text{ mm} \times 3 \text{ mm}$. And, the number of nanoneedles included in the device is estimated to be around 3×10^7 . The inset in Fig. 5 is the corresponding Fowler–Nordheim (F–N) plot of $\ln(J/E^2)$ versus $1/E$, which reveals a linear relationship

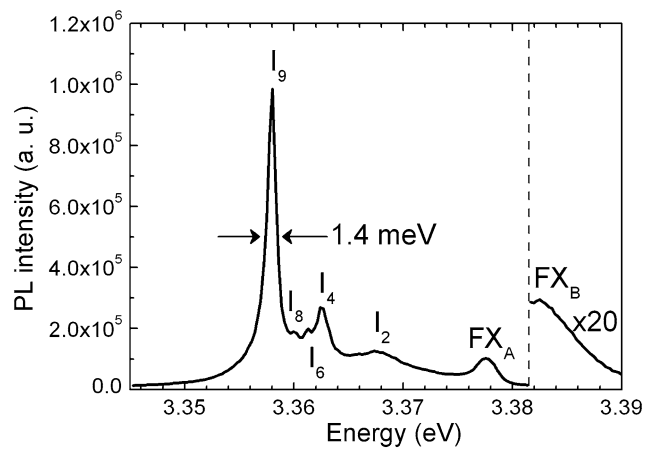


Fig. 4 10 K PL spectrum of near-band edge of ZnO nanoneedle arrays. Peaks were assigned to free excitons (FX_A and FX_B) and excitons bound to neutral donors (I_2 , I_4 , I_6 , I_8 and I_9) [24, 25]

above the turn-on electric field. The results show that the field emission of highly vertically aligned ZnO nanoneedle

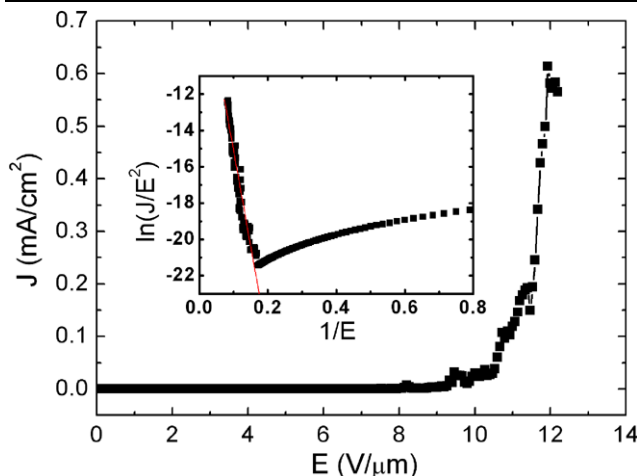


Fig. 5 Plot of field emission current density (J) as a function of applied electric field (E) for highly vertically aligned ZnO nanoneedle arrays with area of $1\text{ mm} \times 3\text{ mm}$. Inset plots $\ln(J/E^2)$ vs. $1/E$, and the solid line presents the linear fitted results

arrays follows the F–N theory closely. As shown in the inset of Fig. 5, the turn-on electric field is $5.9\text{ V}/\mu\text{m}$ (the turn-on field is defined herein as the point at which the slope changes from positive to negative). However, the emission current density reached only about $0.6\text{ mA}/\text{cm}^2$ at an applied field of $12\text{ V}/\mu\text{m}$. Kato et al. [26] reported that the free-carrier concentration of unintentionally doped ZnO layer grown under Zn-rich conditions is about $1 \times 10^{17}\text{ cm}^{-3}$. Therefore, our result probably follows from the fact that the sapphire substrates were insulating and the current flowed laterally through the unintentionally doped ZnO thin film, yielding a large resistance. In addition, the nanoneedles herein also have been unintentionally doped. Heavy n-type doping may reduce the resistivity and the voltage drop along the nanoneedles, and enhanced field emission has been demonstrated in boron-doped carbon nanotubes due to the dopant atoms reducing the work function [27]. The field enhancement factor β of around 793 was calculated from the slope of the F–N plot above the turn-on electric field based on the assumption that the work function $\Phi = 5.3\text{ eV}$ [28, 29]. Our result is comparable to the values for ZnO nanoneedle arrays which were prepared by electrochemical deposition method [12] ($\beta = 758$ at electrodes gap = $200\text{ }\mu\text{m}$) and multiwall carbon nanotubes [30] ($\beta = 830$ at electrodes gap = $125\text{ }\mu\text{m}$).

4 Conclusion

In summary, highly vertically aligned ZnO nanoneedle arrays were grown on wafer-scale catalyst-free c-plane sapphire substrates by PA-MBE at 650°C under high Zn flux conditions. PL measurements revealed that the highly vertically aligned ZnO nanoneedle arrays were of high opti-

cal quality. Additionally, the field emission properties of the highly vertically aligned ZnO nanoneedle arrays were investigated with reference to the F–N law. The turn-on electric field was about $5.9\text{ V}/\mu\text{m}$ with a field enhancement factor β of around 793, which demonstrates potential for applications in future flat display devices at low cost.

Acknowledgements The authors would like to thank the National Science Council of the Republic of China, Taiwan, for financially supporting this research under Contract Nos. NSC 95-2112-M-033-008-MY3 and NSC 98-2112-M-033-003-MY3. The National Nano-Device Lab is appreciated for its support.

References

1. J.T. Hu, T.W. Odom, C.M. Lieber, Acc. Chem. Res. **32**, 435 (1999)
2. Y.Y. Wu, R. Fan, P.D. Yang, Nano Lett. **2**, 83 (2002)
3. E. Comini, G. Faglia, G. Sberveglieri, Z.W. Pan, Z.L. Wang, Appl. Phys. Lett. **81**, 1869 (2002)
4. Y.N. Xia, P.D. Yang, Y.G. Sun, Y.Y. Wu, B. Mayers, B. Gates, Y.D. Yin, F. Kim, Y.Q. Yan, Adv. Mater. **15**, 353 (2003)
5. V.T. Binh, S.T. Purcell, Appl. Surf. Sci. **111**, 157 (1997)
6. Y. Saito, S. Uemura, Carbon **38**, 169 (2000)
7. Z.K. Tang, G.K. Wong, P. Yu, M. Kawasaki, A. Ohmoto, H. Koinuma, Y. Segawa, Appl. Phys. Lett. **72**, 3270 (1998)
8. D.M. Bagnall, Y.F. Chen, Z. Zhu, T. Yao, M.Y. Shen, T. Goto, Appl. Phys. Lett. **73**, 1038 (1998)
9. Q. Zhao, H.Z. Zhang, Y.W. Zhu, S.Q. Feng, X.C. Sun, J. Xu, D.P. Yu, Appl. Phys. Lett. **86**, 203115 (2005)
10. W.I. Park, G.C. Yi, M. Kim, S.J. Pennycook, Adv. Mater. **14**, 1841 (2002)
11. Y.W. Zhu, H.Z. Zhang, X.C. Sun, S.Q. Feng, J. Xu, Q. Zhao, B. Xiang, R.M. Wang, D.P. Yu, Appl. Phys. Lett. **83**, 144 (2003)
12. B. Cao, W. Cai, G. Duan, Y. Li, Q. Zhao, D. Yu, Nanotechnology **16**, 2567 (2005)
13. Z. Zhang, H. Yuan, J. Zhou, D. Liu, S. Luo, Y. Miao, Y. Gao, J. Wang, L. Liu, L. Song, Y. Xiang, X. Zhao, W. Zhou, S. Xie, J. Phys. Chem. B **110**, 8566 (2006)
14. R.C. Wang, C.P. Liu, J.L. Huang, S.J. Chen, Y.K. Tseng, S.C. Kung, Appl. Phys. Lett. **87**, 013110 (2005)
15. S. Muthukumar, H. Sheng, J. Zhong, Z. Zhang, N.W. Emanetoglu, Y. Lu, IEEE Trans. Nanotechnol. **2**, 50 (2003)
16. C.L. Hsu, S.J. Chang, H.C. Hung, Y.R. Lin, C.J. Huang, Y.K. Tseng, I.C. Chen, IEEE Trans. Nanotechnol. **4**, 649 (2005)
17. T.F. Chung, L.B. Luo, Z.B. He, Y.H. Leung, I. Shafiq, Z.Q. Yao, S.T. Lee, Appl. Phys. Lett. **91**, 233112 (2007)
18. Y.W. Heo, V. Varadarajan, M. Kaufman, K. Kim, D.P. Norton, F. Ren, P.H. Fleming, Appl. Phys. Lett. **81**, 3046 (2002)
19. L.C. Tien, D.P. Norton, S.J. Pearton, H.T. Wang, F. Ren, Appl. Surf. Sci. **253**, 4620 (2007)
20. H.J. Ko, T. Yao, Y. Chen, S.K. Hong, J. Appl. Phys. **92**, 4354 (2002)
21. A. Setiawan, Z. Vashaei, M.W. Cho, T. Yao, H. Kato, M. Sano, K. Miyamoto, I. Yonenaga, H.J. Ko, J. Appl. Phys. **96**, 3763 (2004)
22. J.Q. Hu, Q. Li, N.B. Wong, C.S. Lee, S.T. Lee, Chem. Mater. **14**, 1216 (2002)
23. Z.L. Wang, X.Y. Kong, Y. Ding, P.X. Gao, W.L. Hughes, R.S. Yang, Y. Zhang, Adv. Funct. Mater. **14**, 943 (2004)
24. C. Jagadish, S.J. Pearton, Zinc Oxide Bulk, Thin Films and Nanostructures Processing, Properties and Applications (Elsevier, Amsterdam, 2006)

25. S. Müller, D. Stichtenoth, M. Uhrmacher, H. Hofäss, C. Ronning, J. Röder, *Appl. Phys. Lett.* **90**, 012107 (2007)
26. H. Kato, M. Sano, K. Miyamoto, T. Yao, *Jpn. J. Appl. Phys.* **42**, 2241 (2003)
27. J.C. Charlier, M. Terrones, M. Baxendale, V. Meunier, T. Zacharia, N.L. Rupesinghe, W.K. Hsu, N. Grobert, H. Terrones, G.A. Ama-ratunga, *Nano Lett.* **2**, 1191 (2002)
28. C.J. Lee, T.J. Lee, S.C. Lyu, Y. Zhang, H. Ruh, H.J. Lee, *Appl. Phys. Lett.* **81**, 3648 (2002)
29. T. Minami, T. Miyata, T. Yamamoto, *Surf. Coat. Technol.* **108–109**, 583 (1998)
30. J.M. Bonard, J.P. Salvetat, T. Stöckli, L. Forró, A. Châtelain, *Appl. Phys. A* **69**, 245 (1999)